

The Observed Evolution of Galaxy Clustering vs. Epoch-Dependent Biasing Models

M. Magliocchetti¹, J.S. Bagla^{1,2}, S.J. Maddox^{1,3}, O. Lahav^{1,4}

¹*Institute of Astronomy, Madingley Road, Cambridge CB3 0HA*

²*Harvard-Smithsonian Center for Astrophysics, Mail Stop 51, 60 Garden Street, Cambridge, MA 02138, U.S.A.*

³*School of Physics and Astronomy, University of Nottingham, Nottingham, NG7 2RD, UK.*

⁴*Racah Institute of Physics, The Hebrew University, Jerusalem 91904, Israel*

3 December 2017

ABSTRACT

We study the observed evolution of galaxy clustering as a function of redshift. We find that the clustering of galaxies, parameterized by the amplitude of fluctuations in the distribution of galaxies at a co-moving scale of $8h^{-1}$ Mpc, decreases as we go from observations of the local Universe to $z \sim 2$. On the other hand, clustering of the Lyman break galaxies at $z \sim 3$ is very strong, comparable to the clustering of present day galaxies.

However there are three major factors to take into account while comparing clustering measurements coming from various surveys: the so-called “scale-dependence” effect, due to measurements being made at different scales; the “type-selection” effect introduced by the fact that different galaxy surveys select different populations which do not have the same clustering amplitudes; and the Malmquist bias which means that within a given survey the more distant galaxies tend to have brighter absolute magnitudes, and so do not have the same clustering amplitude. We correct for the first two effects and discuss the implications of Malmquist bias on the interpretation of the data at different z . Then we compare the observed galaxy clustering with models for the evolution of clustering in some fixed cosmologies. Correcting for the scale-dependence effect significantly reduces the discrepancies amongst different measurements.

We interpret the observed clustering signal at high redshift as coming from objects which are highly biased with respect to the underlying distribution of mass; this is not the case for $z \lesssim 2$ where measurements are compatible with the assumption of a much lower biasing level which only shows a weak dependence on z . Present observations still do not provide a strong constraint because of the large uncertainties but clear distinctions will be possible when larger datasets from surveys in progress become available. Finally we propose a model-independent test that can be used to place a lower limit on the density parameter Ω_0 .

Key words: galaxies: clustering - galaxies: general - cosmology: theory - large-scale structure

1 INTRODUCTION

It is believed that structures like galaxies and clusters of galaxies formed by accretion of matter onto small inhomogeneities present in the early Universe. The simplest models assume that the distribution of galaxies is directly related to the underlying density distribution and the two distributions evolve in a similar manner. This has provided a key motivation for redshift surveys of galaxies. However, many studies have shown that the relation between galaxy clustering and that of underlying matter is not simple and this relation is, in general, a function of time (Brainerd and Villumsen 1994; Fry 1996; Mo and White 1996; Bagla 1998; Dekel and La-

hav 1998; Tegmark and Peebles 1998; Narayanan, Berlind and Weinberg 1998; Blanton et al. 1998; Colín et al. 1998; Baugh et al. 1999; Kauffmann et al. 1999). These studies deal with the evolution of the clustering of dark matter halos and many factors, including observational selection functions and evolution of stellar populations in galaxies have to be taken into account before these results can be applied to real observations. Some comparisons of models and observations have been carried out (Matarrese et al. 1997; Moscardini et al. 1998) where a large class of models were compared with the available observations.

Models of halo clustering (Mo and White 1996; Bagla

1998) suggest that more massive halos cluster more strongly than halos of lower mass. This follows from the simple model for biasing (Kaiser 1984) in which rare objects cluster more strongly than the more typical objects. If, as observations suggest, the luminosity of a galaxy increases monotonically with the mass of the halo in which it resides, then we expect brighter galaxies to cluster more strongly than fainter galaxies. The same argument also suggests that amongst halos of a given mass, older halos cluster more strongly. If the gravitational clock is synchronised with the stellar clock then we expect early type galaxies to cluster more strongly than late type galaxies. This is seen in simulations (Blanton et al. 1998) that include simple recipes for star formation.

A common conclusion of all theoretical and numerical studies of halo clustering is that the rate of evolution of halo clustering, $D_{halo}(t)$, is always slower than the rate of evolution of clustering in dark matter $D_m(t)$, so that $\dot{D}_{halo}(t) \leq \dot{D}_m(t)$, where the dot represents differentiation with respect to time. These rates are equal only in the limit when all the matter has collapsed into halos.

Turning now to a brief discussion of effects that influence the observed evolution of galaxy clustering, consider a Universe in which the galaxies do not evolve: neither in their stellar content, nor in their distribution in space. So the clustering is fixed in comoving space and galaxies at all redshifts are similar to the ones we see in the local Universe. What will be the observed amplitude of clustering at different redshifts, if we conduct a magnitude limited redshift survey in such a Universe? As nothing is changing as far as galaxies are concerned, the only differences are given by observational selection effects. There are at least two of these: Malmquist bias and K-correction. Let us examine the effect of these two factors separately.

In an apparent magnitude limited survey, we will only see brighter galaxies at high redshifts whereas at lower redshifts we will also see fainter galaxies. Since brighter galaxies tend to cluster more strongly than fainter galaxies (Park et al. 1994; Loveday et al. 1995), the effect of Malmquist bias in our imaginary survey will lead to an apparent increase in the amplitude of clustering with redshift. Also in an apparent magnitude limited sample, the observed clustering amplitude will always exceed the true clustering amplitude of all galaxies at that redshift. This variation with redshift can be avoided by using a cut in absolute magnitude instead of apparent magnitude, but the inferred absolute magnitudes depend explicitly on the assumed values of cosmological parameters. However, without going into any details of dependence on cosmological parameters and models of galaxy evolution, we can conclude that the observed rate of evolution of clustering amplitude is always smaller than the true rate in a magnitude limited survey, the only assumption here being that brighter galaxies cluster more strongly than fainter galaxies: $\dot{D}_{obs}(t) \leq \dot{D}_{true}(t)$.

The effect of K-correction depends strongly on the wave-band used to define the sample. For example, the difference between the rest-frame B band luminosity for ellipticals and irregulars observed in the B band is ~ 4 magnitudes at $z = 1$, but is only ~ 2 magnitudes if they are observed in the I band (Tresse 1999). This effect means that the relative populations of early- and late-type galaxies in a B band selected survey will vary strongly as a function of redshift, preferentially selecting late-types at higher redshift. Since

later-type galaxies cluster less strongly than early types (e.g. Loveday et al. 1995; Hermit et al. 1996; Guzzo et al. 1997; Loveday Tresse & Maddox 1999) a sample defined in the optical will generally tend to underestimate the correlation amplitude at higher redshifts. In the near infra-red the spectral energy distributions of different galaxy types are very similar to each other, and so the K-corrections are very similar. Hence the problem is less significant if we use near infra-red wavelengths to define the sample. Quantifying this effect requires knowledge of the relative fractions of different galaxy populations as a function of redshift, and of how the clustering varies for each population. We plan to tackle this problem in a future paper, but in our present analysis we have simply grouped the various measurements according to the survey selection criteria so that the differences between types are minimized.

This problem could be by-passed if a fixed rest-frame bandpass were used to define the sample, but even this would not take into account the spectral evolution of galaxies. In the real Universe, all galaxies tend to get bluer at higher redshifts, because of stellar evolution, and so the differences between different types of galaxies become smaller. This means that in the real Universe, uncertainties due to different K-corrections will be smaller than in our imaginary Universe.

Another factor which affects the interpretation of the data from various surveys is the ‘‘scale-dependence’’ of the measurements: different surveys sample clustering on different physical scales. Even though the values for the correlation length $r_0(z)$ may be of the order of a few Mpc’s, many surveys (especially those at high redshifts) do not sample scales above $\sim 1 \text{ h}^{-1} \text{ Mpc}$. Since the correlation function is not necessarily a pure power law and the measurements have different slopes, this effect can introduce systematic offsets between the various surveys. To take this into account in this paper, we always compare theoretical predictions to data at the same scale.

This paper presents a compilation of clustering measurements and aims to introduce some simple scenarios for the evolution of clustering in order to understand the different factors which enter into the comparison of data and models. More detailed quantitative discussion on the evolution of clustering will require corrections for all of the effects discussed above, possibly through comparison with a library of models for galaxy formation (e.g. semi-analytical models) convolved with observational selection effects.

The layout of the paper is as follows: section 2 introduces simple analytical models for the evolution of bias with epoch, while section 3 presents the observations and shows the trend of the ‘‘raw’’ data (i.e. with no corrections applied for the effects described in this section) together with simple models for the evolution of clustering. A more detailed analysis of the data, together with our interpretation of the results is given in section 4. Section 5 introduces a model-independent test to place a lower-limit on the density parameter Ω_0 , while section 6 summarises our conclusions.

2 EVOLUTION OF BIAS

Most theoretical models for evolution of galaxy clustering identify galaxies with halos. Here we will describe a few models for the redshift evolution of the bias of halos $b(z)$.

• **No Evolution (B0)** : In this model bias does not change with redshift and remains constant at its present value. This assumption does not have any physical basis and this model serves only as a reference. The bias is defined as

$$b_0 = \frac{\sigma_{8,g}}{\sigma_{8,m}}, \quad (1)$$

where σ_8 is the r.m.s. density fluctuation at $8h^{-1}$ Mpc, subscripts g and m denote galaxies and total underlying mass, respectively and all quantities are evaluated at $z = 0$.

As the halo correlation function evolves at a slower rate than the dark matter one, we expect bias to be higher at high redshifts than at present. Therefore this model should underestimate $\sigma_{8,g}(z)$ at high z .

• **Test Particle Bias (B1)** : This model does not assume anything about the origin of halos, or about their initial distribution. Test particles are distributed through the Universe such that their density contrast is proportional to the density contrast of the total underlying mass. The model describes the evolution of bias for these test particles by assuming that they follow the cosmic flow. It can be shown (Nusser and Davis 1994; Fry 1996; Tegmark and Peebles 1998) that the bias for such test particles evolves as

$$b(z) = 1 + \frac{b_0 - 1}{D(z)}, \quad (2)$$

where $D(z)$ is the linear growth rate for clustering. Here b_0 is the bias for the set of halos/test particles at present epoch (see equation 1). This bias does not depend on the mass of halos and the model works well in the range $0 \lesssim z \lesssim 1$ for CDM like models (Bagla 1998) if the halo distribution is biased. Note that the predicted variation for anti-biased halos ($b_0 < 1$) is not seen in simulations simply because the basic premise of inert, indestructible halos is not correct. This model is also called the *galaxy conserving model* (Matarrese et al. 1997).

• **Merging Model (B2)** : This model (Matarrese et al. 1997) for the evolution of galaxy bias allows halos to undergo dissipative collapse (i.e. merging). It is based on the Mo and White (1996) model for halo bias which was in turn computed, from the formalism of Press and Schechter (1974). The bias is computed for all halos with mass M above a certain threshold M_{min} which is computed by normalizing the effective bias b^{eff} at $z = 0$ to the observed bias. The generic expression for bias of halos of mass $M > M_{min}$ is given by

$$b(M, z) = b_{-1} + (b_0^{eff} - b_{-1})/D(z)^\beta, \quad (3)$$

where the parameters b_0^{eff} and β depend on the choice of M_{min} and the background cosmology. As in the model of Mo and White (1996), there is also some dependence on the formation redshift of halos, which in this case was fixed to a generic z_F . The constant value $b_{-1} = 0.41$ is obtained in the limit $M_{min} \rightarrow 0$.

In the present study, we decided to leave M_{min} as a free parameter (ranging $10^{10} M_\odot \leq M_{min} \leq 10^{13} M_\odot$) so as to allow the objects under consideration to be either transient or to have changed their properties with time (c.f. *transient model* (Matarrese et al. 1997)), and to keep the discussion on a more general level.

As already stated, both the values of b_0^{eff} and β and those for b_0 (and therefore of $\sigma_{8,m}$ through equation 1) are de-

termined by the choice of the cosmological parameters and power spectrum of mass fluctuations. In the following models we will consider three combinations, namely

- I : $\Omega_0 = 1 \quad \Omega_{\Lambda,0} = 0 \quad h_0 = 1 \quad \Gamma = 0.25$
 $\sigma_{8,m}^{lin} = 0.65$
- II : $\Omega_0 = 0.4 \quad \Omega_{\Lambda,0} = 0 \quad h_0 = 0.65 \quad \Gamma = 0.23$
 $\sigma_{8,m}^{lin} = 0.64$
- III : $\Omega_0 = 0.4 \quad \Omega_{\Lambda,0} = 0.6 \quad h_0 = 0.65 \quad \Gamma = 0.23$
 $\sigma_{8,m}^{lin} = 1.07$

The normalization of the linear r.m.s. mass density fluctuations at $8h^{-1}$ Mpc $\sigma_{8,m}^{lin}$ for each power spectrum is chosen to match the four year COBE DMR observations (Bunn and White 1997). The values of the parameters b_0^{eff} and β in equation (3) as functions of different cosmologies and different halo masses are given in Matarrese et al. (1997) and Moscardini et al. (1998). However, much of the discussion is independent of the specific normalization or the shape of the dark matter power spectrum.

We note that biasing is likely to be non-linear, non-local, scale-dependent, type-dependent and stochastic (e.g. Dekel & Lahav 1998; Tegmark & Peebles 1998; Blanton et al. 1998; Narayanan, Berlind and Weinberg 1998), so the models discussed here will give a highly simplified picture of galaxy clustering evolution.

3 OBSERVATIONS

In this section we put together the observations of galaxy clustering from different surveys. In the following we assume that the correlation function has a power-law form $\xi(r, z) = [r/r_0(z)]^{-\gamma}$ at the relevant scales, and hence the index γ and the correlation length r_0 are sufficient to describe it at a given redshift. Most observers quote these numbers and in cases where these were given in proper coordinates, we converted them to the corresponding comoving scales. To transform results between different cosmologies, we use the following expression

$$r_{02}(z) = \left[\frac{h_{01}}{h_{02}} \left(\frac{x_1(z)}{x_2(z)} \right)^{1-\gamma} \frac{P(\Omega_{01}, z)}{P(\Omega_{02}, z)} \frac{F_1(z)}{F_2(z)} \right]^{1/\gamma} r_{01}(z). \quad (4)$$

This equation is derived by requiring that the angular correlation function of a set of galaxies between redshift z and $z + \Delta z$ is the same in different cosmologies. If Δz is small enough for us to assume a constant redshift distribution of objects $N(z)$ then the relativistic Limber equation (Peebles 1980) leads us to equation 4 for a power law correlation function. The relative expressions for the comoving coordinate x and the functions P and F for different geometries are given in Appendix 1 (see also Magliocchetti and Maddox, 1999, Treyer and Lahav, 1996).

To compare different datasets, we will use the r.m.s. fluctuations in the galaxy distribution at the scale of $8h^{-1}$ Mpc, σ_8 .

We relate σ_8 to the other two parameters as (Peebles 1980)

$$\sigma_8(\bar{z}) = \left[\left(\frac{r_0(\bar{z})}{8} \right)^\gamma c_\gamma \right]^{1/2}, \quad (5)$$

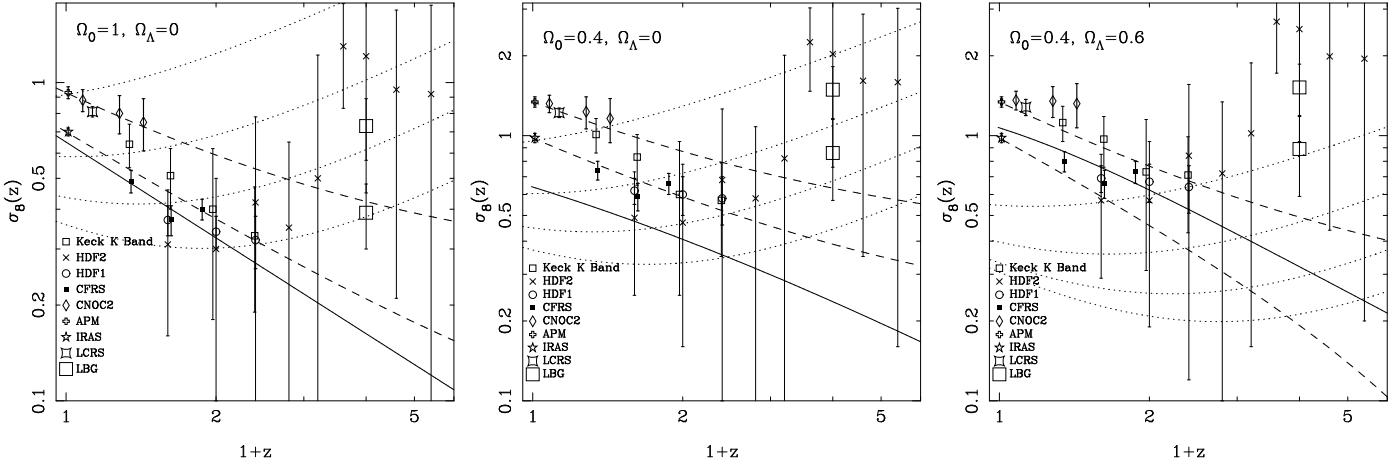


Figure 1. Measurements of σ_8 as a function of redshift respectively for an Einstein-deSitter Universe $\Omega_0 = 1, h_0 = 1$ (left panel), OCDM $\Omega_0 = 0.4, h_0 = 0.65$ (middle panel) and Λ CDM $\Omega_0 = 0.4, \Omega_{\Lambda,0}, h_0 = 0.65$ (right panel). The error bars are the quoted 68% confidence limits or the equivalent taken from the papers cited in the description of surveys used here. The thick line shows the linear rate of growth for dark matter. The dashed curves show evolution as predicted by the test particle model, the two curves are anchored to the APM and the IRAS observations at $z = 0$. The dotted curves show the evolution of bias in the merging model for $10^{10}, 10^{11}, 10^{12}$ and $10^{13}M_{\odot}$ from bottom upwards.

$$c_{\gamma} = \frac{72}{(3-\gamma)(4-\gamma)(6-\gamma)2^{\gamma}}. \quad (6)$$

The list of surveys from which the data points have been taken is given below and in table 1, along with detailed information about the relevant parameters of each survey. These parameters include the median redshift $\langle z \rangle$ of the survey, the number of galaxies N_{GAL} in each survey, the angular coverage, the selection band, the range of absolute magnitudes L (if available) of the objects included in the analysis of clustering and the relative values of γ . We considered the following surveys:

- Stromlo-APM (Loveday et al. 1995).
- IRAS (Saunders et al. 1992).
- Las Campanas (Huan et al. 1996).
- CFRS (Le Fevre et al. 1996).
- HDF₁ (Connolly, Szalay & Brummer, 1998).
- HDF₂ (Magliocchetti & Maddox, 1999).
- Keck K-band (Carlberg et al. 1997).
- CNOC2 (Carlberg et al. 1998).
- LBG₁ (Giavalisco et al., 1998).
- LBG₂ (Adelberger et al., 1998).

The values for $\sigma_8(\bar{z})$ for the three cosmologies presented in section 2 are shown in Figure 1. Note that there are two different points for Lyman break galaxies (LBG) at $z = 3$. These correspond to two different subsamples – one with observed redshifts that can generally be described as the brighter sample, and the other with photometric redshifts. In the first case the amplitude of fluctuations is determined by counts-in-cells (Adelberger et al. 1998) and in the other case it is arrived at through the angular correlation function (Giavalisco et al. 1998). The higher amplitude point corresponds to the sample with redshifts.

In order to guide the eye we also plotted some simple models for the evolution of clustering. Here we assume $\sigma_{8,m}(z)$ to vary with redshift according to linear theory, i.e. we write

$$\sigma_{8,g}(z) = b(z) \sigma_{8,m}^{\text{lin}}(z), \quad \text{with} \\ \sigma_{8,m}(z) = \sigma_{8,m}^{\text{lin}}(z=0) \frac{D(z)}{D(z=0)}, \quad (7)$$

($D(z=0) = 1$ by definition), and $b(z)$ given by equations (1-3). The thick line shows the linear rate of growth for dark matter. It is clear that within any given survey, the amplitude of fluctuations does not fall as rapidly as the linear rate. This is encouraging because according to the arguments outlined in the introduction, the observed rate of evolution should always be smaller than the rate of evolution of mass. The dashed curves show evolution as predicted by the test particle model (B1), the two curves are anchored to the APM and the IRAS observations at $z = 0$. The dotted curves show the evolution of bias in the merging model (B2) for $10^{10}, 10^{11}, 10^{12}$ and $10^{13}M_{\odot}$ from bottom upwards.

The basic pattern followed by the amplitude of clustering, even though it is masked to some extent by large error bars and differences in different datasets, is that - independent of the cosmological model - at low redshifts, $\sigma_{8,g}$ decreases with increasing redshift, reaches a minima around $z = 2$ and then rises again at higher redshifts. This type of variation has been seen for dark matter halos in N-body simulations (see e.g Jenkins et al. 1998), but given the observational complications discussed earlier, these simulations cannot be directly compared to the observational data.

Table 1. Summary of the properties of each survey.

Survey	$\langle z \rangle$	N_{GAL}	Angular Coverage	Selection band	Absolute Magnitude	\bar{z}	γ
IRAS	≤ 0.1	9080	$ b > 10^\circ$	$F_{60} \leq 0.6Jy$?	~ 0.06	1.57 ± 0.03
Stromlo-APM	0.06	1757	4300 deg ²	$b_j \leq 17.5$	$-22 \leq L_B \leq -15$	~ 0.05	1.71 ± 0.05
Las Campanas	0.1	19558	700 deg ²	$R \leq 17.75$	$-23 \leq L_R \leq -18$	0.13	1.85 ± 0.05
CNOC2	0.36	~ 2000	$40 \times 9' \times 8'$	$R \leq 24$	$L_R \geq -20$	0.08	1.8 ± 0.1
CNOC2	0.36	~ 2000	$40 \times 9' \times 8'$	$R \leq 24$	$L_R \geq -20$	0.28	1.8 ± 0.1
CNOC2	0.36	~ 2000	$40 \times 9' \times 8'$	$R \leq 24$	$L_R \geq -20$	0.43	1.8 ± 0.2
CFRS	0.56	591	$5 \times 10' \times 10'$	$17.5 \leq I_{AB} \leq 22.5$	$-21.5 \lesssim L_B \lesssim -18.5$	0.35	1.64 ± 0.05
CFRS	0.56	591	$5 \times 10' \times 10'$	$17.5 \leq I_{AB} \leq 22.5$	$-22.0 \lesssim L_B \lesssim -19.5$	0.62	1.64 ± 0.05
CFRS	0.56	591	$5 \times 10' \times 10'$	$17.5 \leq I_{AB} \leq 22.5$	$-22.5 \lesssim L_B \lesssim -21.0$	0.87	1.64 ± 0.05
Keck K-band	0.7	248	27 arcmin ²	$K \leq 20$	$L_K \geq -21.5$	0.34	1.8
Keck K-band	0.7	248	27 arcmin ²	$K \leq 20$	$L_K \geq -23.5$	0.62	1.8
Keck K-band	0.7	248	27 arcmin ²	$K \leq 20$	$L_K \geq -23.5$	0.97	1.8
Keck K-band	0.7	248	27 arcmin ²	$K \leq 20$	$L_K \geq -23.5$	1.39	1.8
HDF ₁	1	926	5 arcmin ²	$I_{AB} \leq 27$?	0.6	1.8
HDF ₁	1	926	5 arcmin ²	$I_{AB} \leq 27$?	1.0	1.8
HDF ₁	1	926	5 arcmin ²	$I_{AB} \leq 27$?	1.4	1.8
HDF ₂	1.6	946	4 arcmin ²	$AB(8140) \leq 28$?	0.6	1.8
HDF ₂	1.6	946	4 arcmin ²	$AB(8140) \leq 28$?	1.0	1.8
HDF ₂	1.6	946	4 arcmin ²	$AB(8140) \leq 28$?	1.4	1.8
HDF ₂	1.6	946	4 arcmin ²	$AB(8140) \leq 28$?	1.8	1.8
HDF ₂	1.6	946	4 arcmin ²	$AB(8140) \leq 28$?	2.2	1.8
HDF ₂	1.6	946	4 arcmin ²	$AB(8140) \leq 28$?	2.6	1.8
HDF ₂	1.6	946	4 arcmin ²	$AB(8140) \leq 28$?	3.0	1.8
HDF ₂	1.6	946	4 arcmin ²	$AB(8140) \leq 28$?	3.6	1.8
HDF ₂	1.6	946	4 arcmin ²	$AB(8140) \leq 28$?	4.4	1.8
LBG ₁	3	871	$9 \times \sim 9' \times 9'$	$R \leq 25.5$?	3.0	1.98 ± 0.3
LBG ₂	3	268	$6 \times \sim 9' \times 9'$	$R \leq 25.5$?	3.0	1.8

4 INTERPRETATION

Given the general trend shown in Figure 1, we have to address the following questions: (1) Why does the observed clustering vary across datasets? (2) Is it possible to scale different datasets to make a self-consistent dataset, and then study evolution within that superset? (3) Can we constrain any of the models using this data?

There are significant discrepancies between the amplitude of clustering in different surveys even where they sample the same redshift intervals. To some extent these discrepancies are intrinsic because different surveys sample different populations of galaxies. Some differences are introduced by the extent to which the luminosity function is probed, i.e. in one survey the limiting magnitude may allow one to probe galaxies much fainter than L^* and in another case the limiting magnitude may be comparable to L^* . Since different surveys measure clustering at different scales, and many of them extrapolate the values for $r_0(z)$ on scales bigger than the areas actually covered by the surveys themselves (see table 1), further differences are introduced if the galaxy correlation function is not a true power law in the range of scales between the scale of measurement and $8h^{-1}$ Mpc.

All these effects are very likely to “bias” the different measurements with respect to each other. In this section we tackle these issues one by one, in order to correct the data for their effects so to obtain “unbiased” sub-sets of measurements compatible with each other.

4.1 Scale Dependence

As already mentioned in the previous sections and as shown in table 1, different surveys cover areas of the sky which vary greatly in size from one survey to another. This problem of sampling objects on different scales is likely to introduce a relative bias amongst clustering measurements coming from different surveys. In fact many of these studies quote values for the clustering length $r_0(z)$ which have been obtained by extrapolating the power-law trend of $\xi(r, z)$ to scales much larger than the physical scales of the surveys. In order to correct for this effect we write the bias as

$$b^2(\bar{r}, z) = \frac{\xi_g(\bar{r}, z)}{\xi_m(\bar{r}, z)}, \quad (8)$$

where ξ_m and ξ_g respectively are the mass-mass and galaxy-galaxy correlation function and \bar{r} is some fiducial scale length. Note that by writing the bias as an explicit function of \bar{r} which is different for each survey, this approach corrects for the “scale effect”, since it compares theoretical quantities and measurements evaluated at the same scale.

We start by evaluating the mass-mass correlation function $\xi_m(\bar{r}, z)$. Throughout this section we will use the notations adopted in Peacock (1997). We start with a (dimensionless) primordial power-spectrum of the form $\Delta_{lin}^2(k) \propto k^{n+3} T_k^2$ (with $n = 1$ for CDM models). The transfer function for CDM family of models is the one given by Bardeen et al. (1986):

$$T(k) = \frac{\ln(1 + 2.34q)}{2.34q} \times [1 + 3.89q + (16.1q)^2 + (5.46q)^3 + (6.71q)^4]^{-1/4}, \quad (9)$$

where $q = (k/h)/\Gamma \text{ Mpc}^{-1}$ and the shape parameter Γ is related to the present-day matter parameter Ω_0 and the baryonic fraction Ω_{0b} via $\Gamma = \Omega_0 h \exp[\Omega_{0b} - \sqrt{h/0.5} \Omega_{0b}/\Omega_0]$ (Sugiyama, 1995). The normalization of the power-spectrum is fixed by specifying the values of σ_8^{lin} (see section 2), according to the expression:

$$(\sigma_8^{\text{lin}})^2 = \int \Delta_{\text{lin}}^2(k) \frac{dk}{k} \frac{9}{(kR)^6} [\sin kR - kR \cos kR]^2 \quad (10)$$

In order to go from the linear power-spectrum $\Delta_{\text{lin}}^2(k)$ to the non-linear case, Peacock & Dodds (1994, 1996), following an approach originally introduced by Hamilton et al. (1991), assumed there is a universal fitting function F relating the two according to the expressions:

$$\begin{aligned} \Delta^2(k) &= F[\Delta_{\text{lin}}^2(k_0)], \\ k_0 &= [1 + \Delta^2(k)]^{-1/3} k, \end{aligned} \quad (11)$$

where k_0 and k are respectively the linear and non-linear wavenumber and F is given by:

$$F(x) = x \left[\frac{1 + B\beta x + [Ax]^{\alpha\beta}}{1 + ([Ax]^{\alpha} g(\Omega_0)^3 / [Vx^{1/2}])^\beta} \right]^{1/\beta} \quad (12)$$

(see Peacock & Dodds (1996) for the values of the parameters in equation 12). $g(\Omega_0)$ is a suppression factor which measures the rate of growth of clustering in generic cosmologies relative to the growth in an Einstein-de Sitter Universe. Lahav et al. (1991) and Carrol, Press & Turner (1992) found that this quantity can be almost exactly approximated by

$$g(\Omega_0, \Omega_{\Lambda,0}) = \frac{5}{2} \Omega_0 \left[\Omega_0^{4/7} - \Omega_{\Lambda,0} + (1 + \Omega_0/2) \left(1 + \frac{\Omega_{\Lambda,0}}{70} \right) \right]^{-1}. \quad (13)$$

The above formulae were given in Peacock & Dodds (1996) and Peacock (1997) for $z = 0$. However Moscardini et al. (1997) argue that they all apply to any cosmic epoch z , as long as one replaces g by $g(z)$, and interpret the quantity x as the linear power-spectrum at epoch z :

$$x = \Delta_{\text{lin}}^2(k_0, z) = \Delta_{\text{lin}}^2(k_0) (1+z)^{-2} [g(z)/g(0)]^2. \quad (14)$$

Replacing g by $g(z)$ implies writing both Ω and Ω_{Λ} as a function of redshift. Their expressions have been taken from Lahav et al. (1991) and obviously depend on the underlying cosmology:

$$\begin{aligned} \Omega(z) &= \Omega_0 (h/h_0)^{-2} (1+z)^3 \\ \Omega_{\Lambda}(z) &= \frac{\Lambda c^2}{3h^2}, \end{aligned} \quad (15)$$

where Λ is the cosmological constant which does not vary with time, and

$$h(z) = h_0 \left[\Omega_0 (1+z)^3 - (\Omega_0 + \Omega_{\Lambda,0} - 1)(1+z)^2 + \Omega_{\Lambda,0} \right]^{1/2} \quad (16)$$

Now that we have all the theory in place, we can finally evaluate the evolution of the spatial two-point correlation function $\xi(r, z)$ with time. Note that $\xi(r, z)$ is related to the power-spectrum $\Delta^2(k, z)$ via the expression:

$$\xi(r, z) = \int \Delta^2(k, z) \frac{\sin kr}{kr} \frac{dk}{k} \quad (17)$$

In order to compare theoretical models with data, $\xi(\bar{r}, z)$

has been obtained for all the redshifts sampled by different surveys. The fiducial length \bar{r} has been chosen to be $r_{max}/2$, where r_{max} is the upper limit of the range of scales used to measure the clustering signal within each survey. This choice, even though somewhat ‘‘ad hoc’’, seems plausible given that the measurements go from about $r = 0$ to r_{max} , and this gives an effective radius $\sim r_{max}/2$. A more exact analysis would have to take into account the actual bin steps, weighting and fitting procedure used in deriving ξ for each survey, but since we were only interested in the relative scalings, we kept it to this simple approximation. Note that the values of r_{max} (and therefore of \bar{r}) vary both with redshift and cosmology and correspond to scales that range from linear to highly non-linear (see Figure 2). In the cases where the 3-d clustering was obtained by deprojecting the angular (2-d) correlation function $w(\theta)$ (as for instance in the HDF points), the value of r_{max} was obtained via $r = \theta_{max} x$, with θ_{max} maximum angular scale and x comoving coordinate, whose expressions for different cosmologies are given in Appendix A. We repeated this analysis for the three cosmologies introduced in section 2.

Figure 2 shows the theoretical predictions for the spatial two-point correlation function $\xi(\bar{r}, z)$ at different redshifts and compares them with the respective data. Each panel corresponds to a different survey (an exception has been made for the HDF in order not to overcrowd the relative panel) and the different curves show the predictions for ξ at the redshifts \bar{z} quoted for each of their clustering measurements; the lower curves are for higher z 's.

The points show $\xi(\bar{r}, z)$ derived from the observations assuming a power-law form $\xi(\bar{r}, z) = [\bar{r}/r_0(z)]^{-\gamma}$. The values of γ are directly observed, as listed in table 1 and $r_0(z)$ is derived for each cosmology from expressions (4) and (5). Note that the assumption of a power-law form for ξ is justified by the small areas covered by most of the surveys. In the case of wide-area surveys (such as Stromlo-APM and IRAS) \bar{r} has been fixed to a standard value of 10 Mpc, independent of cosmology. Different symbols correspond to different surveys. In the HDF panels crosses indicate the results from Magliocchetti & Maddox (1999) (HDF₂), while empty circles are for Connolly, Szalay & Brummer (1998) (HDF₁). In the LBG panel the higher point is taken from Adelberger et al. (1998). Figure 2 shows the great spread in the scales sampled by different surveys ranging from a few tenths to $\gtrsim 10$ Mpc. It is also possible to note that even within the same survey (e.g. HDF and LBG), different analysing techniques measure different scales. As we will show later in this section, this scale effect can partially explain the apparent discrepancy amongst results quoted for similar sets of data.

4.2 Populations

Different surveys in general sample different populations of objects; this is due to both the selection criteria and the redshift range sampled by the survey. Objects selected in the UV band will be dominated by star-forming galaxies, while for instance, B band selected objects will give mix of early and late-type galaxies. At higher redshifts the population mix sampled by a survey will also depend on z since the rest-frame pass band is shifted towards the blue. For example a survey which selects objects in the I-band will contain many early-type galaxies at low z , but for $z \gtrsim 1.5$

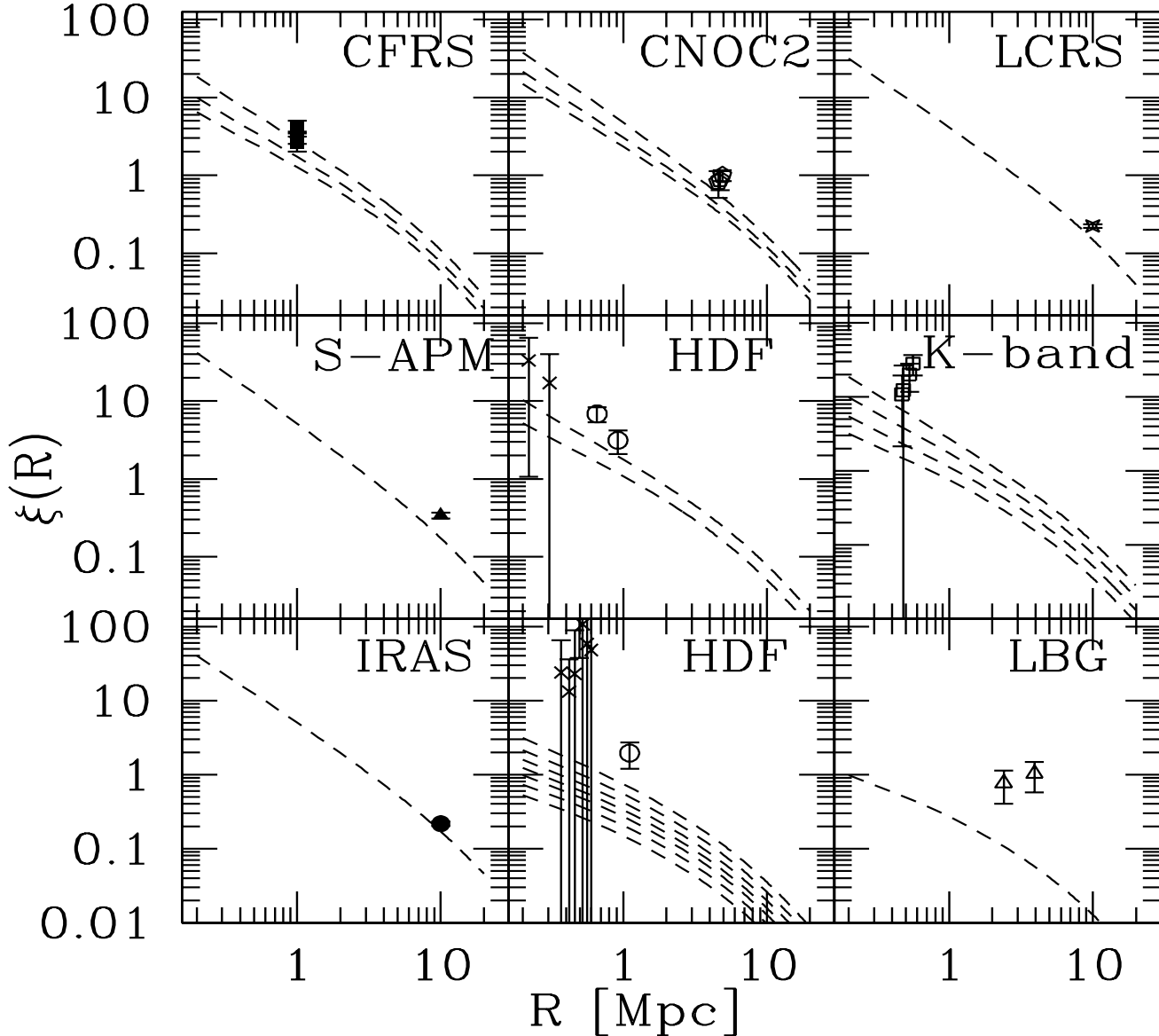


Figure 2. Theoretical predictions for the spatial two-point correlation function $\xi(R)$ at different redshifts and for an Einstein-de Sitter Universe. Each panel corresponds to a different survey and the dashed lines indicate the models obtained for those redshifts \bar{z} 's which have available measurements of $r_0(\bar{z})$ (or alternatively of $\sigma_8(\bar{z})$, see table 1). Lower lines correspond higher redshifts. The points show the values for $\xi(R)$ obtained from the data in the assumption of a power-law form for the correlation function, where R is half the size of the maximum scale used to derive the clustering measurements, representing the scale used to determine r_0 . Different symbols correspond to different surveys. In the HDF panels crosses indicate the results from Magliocchetti & Maddox (1999) (HDF₂), while empty circles are for Connolly, Szalay & Brummer (1998) (HDF₁). In the LBG panel the higher point is taken from Adelberger et al. (1998).

the observed I-band corresponds to the rest-frame UV band, and so the sample will be dominated by star-forming galaxies. This also implies that, even within the same survey, the galaxy population that is sampled depends strongly on the redshift.

Since late-type/star-forming galaxies cluster more weakly than early-type ones (e.g Loveday et al. 1995; Hermit et al. 1996; Guzzo et al. 1997), the changes in the galaxy population must be taken into account when comparing the clustering measurements from different surveys and different redshifts.

As a simple first step to minimizing this effect we di-

vided our sample into different populations, according to the rest-frame selection band. The Stromlo-APM survey samples galaxies in the rest B-band (see table 1) as it does the Las Campanas redshift survey (LCRS, objects selected in the observed R-band at a median redshift $\bar{z} = 0.13$) and the CNOC2. The same holds for both the CFRS survey (I-band selected objects at $0.3 \lesssim z \lesssim 1$) and the HDF for $z \lesssim 1.4$. We will denote the objects selected by these surveys with the collective name of *blue*. At higher redshift the observed I-band shifts into the rest-frame UV band so that, for $z \gtrsim 1.4$, the population sampled by the HDF will be dominated by star-forming galaxies. The selection criteria

of both IRAS and Lyman-Break galaxies also lead to samples dominated by galaxies undergoing star-formation. We will call these objects *star-forming*. The Keck K-band survey selects objects in the near-IR, which for $0.3 \lesssim z \lesssim 1.4$ corresponds to a rest-frame R-band. We therefore expect the populations sampled to be mainly early-type (*red*) galaxies.

Now that we have made this division into different populations according to their star-forming activity and therefore their colours, we can go back to the issues of the evolution of galaxy clustering and the redshift evolution of bias. In more detail, for each of the three populations we have then evaluated the quantity $b(\bar{r}, z) = \sqrt{[\xi_g(\bar{r}, z)/\xi_m(\bar{r}, z)]}$, as explained in section 4.1.

Figure 3 shows the trend of $b(z)$ as a function of $(1+z)$, respectively for blue (left panels), red (middle panels) and star-forming galaxies (right panels). Different symbols correspond to different surveys and are the same as in figure 2. Once again the upper LBG point (empty triangle) is taken from Adelberger et al. (1998). The upper panels are for an Einstein-de Sitter Universe ($\Omega_0 = 1, h_0 = 1$), the middle panels for open cosmologies ($\Omega_0 = 0.4, h_0 = 0.65$) and the lower panels correspond to flat geometries with non-null cosmological constant ($\Omega_0 = 0.4, \Omega_{\Lambda,0} = 0.6, h_0 = 0.65$).

There are many interesting features to note in Figure 3. The first is the trend of points at low redshift ($z \lesssim 1.5$). The large spread amongst the different surveys seen in Figure 1 is much reduced after renormalizing the amplitude according to the scale sampled by each survey. Panels on the left-hand side of Figure 3 show the corrected results in excellent agreement with each other. This good agreement also suggests that there is little dependence of bias on scale.

The systematic higher clustering amplitude in the Keck K-band survey as compared to other surveys (see middle panels in Figure 3) can now be explained as due to different clustering properties of different populations. In more detail the results show, as expected from local measurements, that early-type objects cluster more strongly than late-type ones.

In Figure 3 we have also plotted some theoretical predictions for the evolution of bias with redshift. The solid lines correspond to the test-particle model (B1), described by equation (2). Note that the value of the quantity $b_0 = \sigma_{8,g}/\sigma_{8,m}$ (where in this case $\sigma_{8,m}$ is the non-linear r.m.s. mass density fluctuation at $8h^{-1}$ Mpc, as calculated from the models described in section 4.2) varies for different populations. For the models we use a different value of $\sigma_{8,g}$ for each galaxy type, with star-bursting galaxies being less clustered than quiescent galaxies with old stellar populations. We estimate the amplitudes $\sigma_{8,g}$ from the values of r_0 measured for three subsamples from Stromlo-APM survey (Loveday, Tresse & Maddox, 1999): for galaxies with no emission lines (red objects) $\sigma_{8,g} = 1.13$; galaxies with weak emission (blue galaxies) $\sigma_{8,g} = 0.93$; and $\sigma_{8,g} = 0.66$ for galaxies with strong emission lines (star-forming galaxies).

The dashed lines correspond to the merging model for the evolution of bias with z (B2), with lower curves corresponding to lower halo-masses ($10^{11}M_\odot \leq M_{min} \leq 10^{13}M_\odot$, see section 2). Note that neither the B1 nor the B2 curves have been anchored to any $z = 0$ point.

At low redshift, quite independent of the cosmology, the B1 models seem to provide a reasonably good fit to the data, both in the case of blue and early-type objects, even though we cannot rule out the constant bias model

as a possible description (B0 - equation 1, lines parallel to the x axis, not shown in the figure). This is also seen in the analysis of the clustering of radio galaxies (e.g. Magliocchetti et al. 1999); in this case the mean redshift for the clustering measurements is about $z \sim 1$. Even though the data cannot distinguish between constant bias (B0) models and models with bias linearly evolving with redshift (B1), it is clear that the clustering measurements obtained for the radio sample in such a redshift range are in conflict with the predictions obtained from the merging (B2) model.

At higher redshifts ($z \gtrsim 2$) though, both the constant bias and the test particle model grossly fail to describe the data which show very high values for $b(z)$. Note that in this redshift range we have measurements only for star-forming objects, therefore it is impossible to state whether this rise in the level of biasing is always true for $z \gtrsim 2$, independent of the population, or only holds for star-forming galaxies. Although the match is not perfect, the merging model correctly describes the trend of the data (and also matches the IRAS points), with lower halo-masses ($M_{min} = 10^{12}M_\odot$) required for an Einstein-de Sitter Universe and higher halo-masses ($M_{min} = 10^{13}M_\odot$) for low-density models (independent of $\Omega_{\Lambda,0}$).

4.3 Malmquist bias

Now we turn to a discussion of the selection effects, namely the Malmquist bias and K-correction.

Although it is not possible to correct for the Malmquist-bias and K-correction, models can be made to allow for their effects. In a detailed model (e.g. by using the semi-analytic approach; (Kauffmann et al. 1999; Baugh et al. 1999; Somerville & Primack 1998)), these selection effects can be convolved with the model and direct comparison can be made with the observations. However, these models contain a large number of parameters and the gain in details is accompanied by a loss of intuitive understanding. In order to keep the discussion simple and independent of model parameters, we will not use this approach here.

Instead, by dividing the objects into different populations we minimize the K-correction problem, because objects belonging to the same population are likely to have similar spectra, and so have similar K-corrections.

As already mentioned in the introduction, more luminous galaxies found to cluster more strongly (Park et al. 1994; Loveday et al. 1995) than fainter ones. Therefore, for the apparent magnitude selected samples in Figure 3 we would expect to see an increase of the clustering introduced by the Malmquist bias at higher z 's. The CFRS measurements are based on all galaxies brighter than the apparent magnitude limit of the survey, and so the points sample objects with increasing absolute magnitudes as one goes to higher redshifts. We can see a hint of the expected Malmquist effect in these points in that the third bin (centred at $z \simeq 0.87$) shows a slight increase in clustering amplitude, and includes only galaxies brighter than L_B^* (see table 1). However this is at a very low significance level. On the other hand the measurements from the CNOC2 and the Las Campanas surveys are based on sub-samples of galaxies with a cut-off in absolute magnitude (respectively $L_R \geq -20$ and $-23 \leq L_R \leq -18$, and so should not show this effect.

In the Keck K-band survey (panels in the centre of Fig-

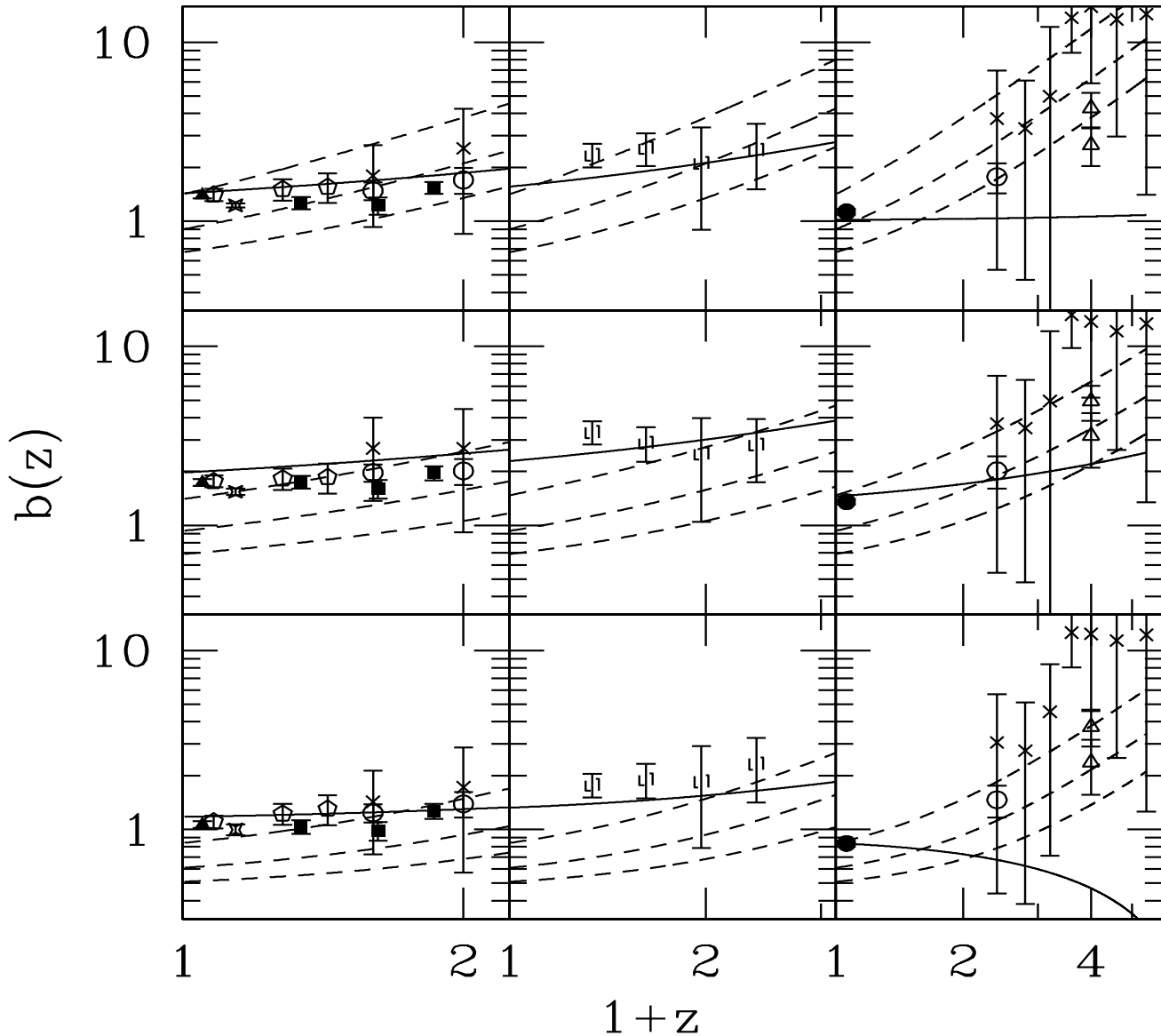


Figure 3. Trend of the bias $b(z)$ as a function of redshift for different populations of objects. Left panels correspond to blue objects, middle panels to red objects and right panels to star-forming galaxies. Symbols are the same as in figure 2. Results have been obtained for an Einstein-de Sitter Universe (top), open Universe (centre) and flat Universe with a cosmological constant (bottom). Lines indicate theoretical models for the evolution of bias as explained in section 2. Solid lines represent the test-particle (B1) model, while the dashed lines are for the merging (B2) model with $M_{min} = 10^{11}, 10^{12}$ and $10^{13} M_{\odot}$, lower curves corresponding to lower halo-masses (see text for details).

ure 3), clustering measurements have been obtained for all the galaxies respectively with $L_K \geq -23$ in the three higher redshift bins and with $L_K \geq -21.5$ in the lower redshift range. We therefore expect the lower- z point to underestimate the clustering with respect to the results for higher z 's and brighter absolute magnitudes. However, given that $L_K^* \sim -25 + 5 \log(h_{50})$, even for $L_K \geq -23.5$, all the galaxies still sit on the flat faint-end of the luminosity function. Since Malmquist bias is likely to be important only for luminosities $\gtrsim L^*$, we argue that the effect should be small in this case.

Unfortunately we do not have reliable information on the absolute luminosities of objects in the HDF because the

K-corrections are highly uncertain, particularly for $z \gtrsim 1$. However, at low redshift ($z \lesssim 1.4$), the faint apparent magnitude limit suggests that all galaxies will be below L^* , and so Malmquist bias should not play an important role. This is consistent with the trend shown by the data in Figure 3 (left panels). At higher redshift the galaxies in the sample are brighter than L^* , therefore we might expect Malmquist bias to be more important, so that the clustering amplitude would increase with increasing redshift as seen in the data.

It would be possible to quantify the Malmquist bias effect by converting the absolute luminosity limit for each subset of galaxies to an equivalent mass limit and hence find the expected clustering amplitude for each redshift. However the

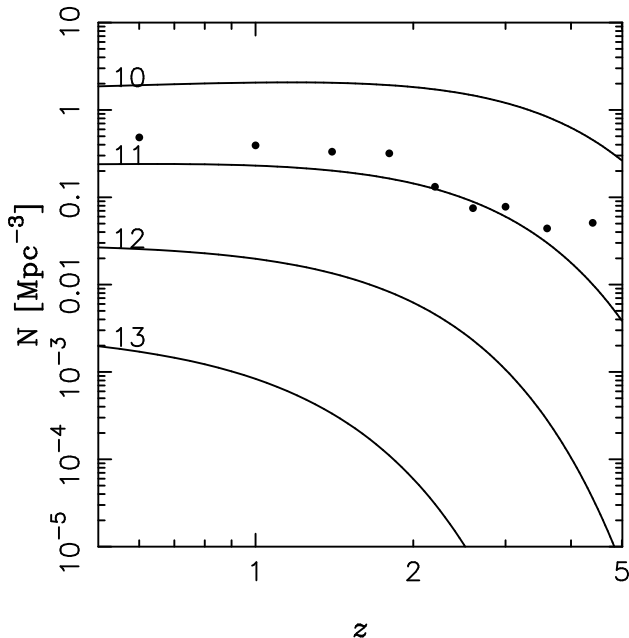


Figure 4. The estimated comoving galaxy space density as a function of redshift. The points show the estimates for the HDF galaxies as used in the clustering measurements. The lines show the Press-Schechter prediction for the density of halos with mass greater than $M_{min} = 10^{10}, 10^{11}, 10^{12}$ and $10^{13} M_{\odot}$, as labelled. We applied the standard Press-Schechter formalism using the cosmology and power spectrum from our model I. The data at $z \gtrsim 3$ are almost certainly affected by random errors, because the space density implies a low M_{min} , whereas the clustering implies a very high M_{min} (see Figure 3).

K-corrections, and hence the derived absolute magnitudes, are highly uncertain at these redshifts. Also the mass-to-light ratio is unknown at high redshift, and given the rapid evolution of stellar populations at $z < 1$, it is likely to be very different to local galaxies. An alternative way to tackle this problem is to consider the space density of objects. In models based on high peak biasing, rarer objects correspond to higher masses, which are more strongly clustered. Hence a comparison between the observed and predicted comoving space-density of galaxies allows us to estimate the effective M_{min} for each redshift bin, independent of uncertainties in the absolute magnitudes. This should provide a more robust approach to quantifying the Malmquist bias.

In Figure 4 the points show the observed mean density for each HDF redshift bin, estimated as $\bar{N} = N_{\Delta z}/V$, where V is the comoving volume in each bin assuming an Einstein-de Sitter Universe. Note that, as expected, there is a clear trend for the space-density to decrease with increasing redshift, although the decrease is not very strong, even at high redshift. The lines show the space density of haloes of mass greater than $M_{min} = 10^{10}, 10^{11}, 10^{12}$ and $10^{13} M_{\odot}$ predicted from the standard Press-Schechter formalism with the power spectrum as in our model I. For $z \lesssim 2$ the points are consistent with a fixed halo mass $\sim 5 \times 10^{10} M_{\odot}$. For $2 \lesssim z \lesssim 4$ there is a hint that M_{min} may rise to $\sim 10^{11} M_{\odot}$, but the uncertainties are large, and for $z \gtrsim 4$ the apparent decrease is not significant. The merging model (B2) introduced by Matarrese et al. (1997) and Moscardini et al. (1998) predicts the evolution of bias with redshift, according to the mass of

the halos. Thus we can compare directly to the model (B2) (dashed lines in the panels on the right-hand side of Figure 3) with a minimum halo mass $M_{min}(z)$ which is roughly constant or slightly increasing with at higher redshifts (see also Arnouts et al. 1999).

5 CONSTRAINTS ON Ω_0

The rate of evolution of the galaxy correlation function with redshift has been used to estimate Cosmological parameters (Peacock 1997). This approach assumes that the bias does not have any scale dependence, and, it does not vary significantly in time. However, recent studies have questioned this approach and have shown that the time evolution of bias is very important, even if we can choose to ignore its scale dependence at large scales. The most remarkable manifestation of the time evolution of bias are the Lyman break galaxies, that have a clustering amplitude comparable to present day galaxies. The models of bias evolution discussed in section 2 also suggest that the time evolution of bias is very important.

In principle, it is possible to use the models of bias along with the observations to see if the observed redshift evolution of clustering is consistent with a given model or not. However, this approach requires the power spectrum for density fluctuations as an input, and hence is model dependent.

We propose a simple test to derive a lower limit on Ω_0 . We make use of the fact that in all realistic scenarios, bias always increases as we go to higher redshifts. This monotonic increase in bias implies that the galaxy correlation function will evolve at a slower rate than the correlation function of dark matter, i.e. $\dot{D}_{gal}(z) \leq \dot{D}_m(z)$. $D_m(z)$ depends only on Ω_0 (and $\Omega_{\Lambda,0}$), and evolves at a slower rate for lower Ω_0 . If we compute the allowed values of $\dot{D}_{gal}(z)$ in a given survey, and we get a firm lower limit on this rate, then we can rule out those cosmologies that predict $\dot{D}_m(z) < \dot{D}_{gal,obs}(z)$. *We would like to stress, that this method is completely model independent if used at large/linear scales.*

To further illustrate this idea, we have plotted the best fit points for CFRS and CNOC2 surveys on the Ω_0 - σ_8 plane in figure 5. Thick lines show the confidence limits at the 68% level. The error bars at this confidence level are too big to be of much use. We have not shown data from any other survey listed in this paper because the error bars for those are even larger. However, to demonstrate what can be achieved by the next generation surveys, like 2DF (Maddox 1998), Sloan (Kim et al. 1999) and VIRMOS (Garilli et al. 1999) which will have many more galaxy redshifts, we have shown the contours for error bars reduced by a factor 5. In this case, one may begin to rule out interesting regions of the parameter space.

This test is more effective at lower redshifts as the difference in the growth rate in different cosmologies is more striking. Thus surveys like Sloan and 2DF may provide some useful constraints through this test.

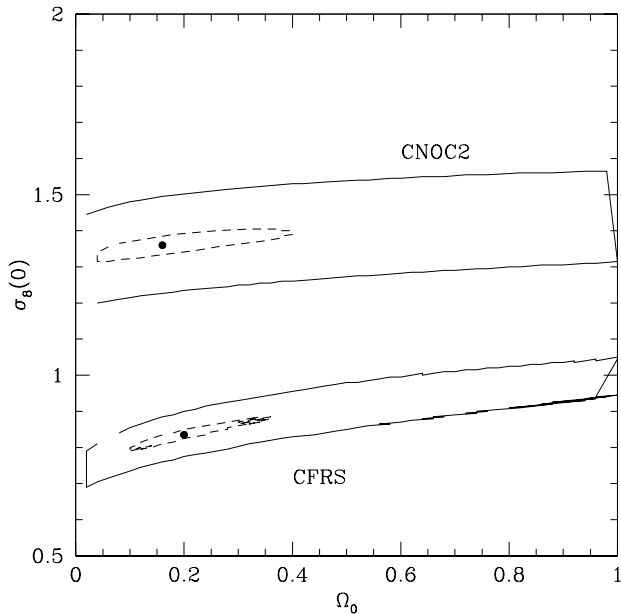


Figure 5. This figure shows the best fit values of Ω_0 and $\sigma_{8,g}(0)$ for CFRS and CNOC2 surveys assuming an open universe with $\Omega_{\Lambda,0} = 0$. The 68% confidence limits are shown as thick lines. Dashed lines show the same if error bars are reduced to 1/5 of their present size. Allowed values for Ω_0 lie on the right-hand side of the diagram. See text for details.

6 CONCLUSIONS

We have presented a detailed analysis of the evolution of galaxy clustering with redshift, specifically aimed at constraining epoch-dependent models for the bias.

As a first step we put together all the available measurements from different surveys, covering $z \simeq 0$ to $z \simeq 4.5$, and we calculated the values for the r.m.s galaxy fluctuation density on a $8h^{-1}$ Mpc scale, $\sigma_{8,g}$. This has been repeated for different cosmologies. We find that the amplitude of galaxy clustering shows a general trend of decreasing at redshifts $z < 2$ and increasing beyond that.

The amplitudes for different surveys show a remarkable scatter between each other, and there are several factors which might be responsible for this. First is the “scale-dependence” problem, coming from the fact that the various surveys measure clustering at different scales. Second is that different surveys select different populations of objects which do not have similar clustering amplitudes. Third is the Malmquist bias, since brighter objects cluster more strongly than fainter ones. By using the Peacock & Dodds (1994, 1996) models for non-linear evolution of the power-spectrum $P(k, z)$ (and consequently of the two-point correlation function $\xi(r, z)$), we corrected for the scale-dependence effect and obtained values for the bias written as $b^2(\bar{r}, z) = \xi_g(\bar{r}, z)/\xi_m(\bar{r}, z)$, where \bar{r} is half of the maximum scale used within each survey to work out estimates on the clustering amplitude. Note that this approach can in principle also show a dependence of bias on scale. We allowed for the population selection effect by dividing the objects into three categories, according to the rest-frame pass band of their selection (roughly corresponding to their star-forming activity) and analyzing the evolution of clustering for each

of these populations separately. We also considered the expected variations introduced by the Malmquist bias.

We find that the main cause for the scatter amongst different surveys is the scale-dependence problem. Renormalizing the amplitudes according to the physical scale at which each measurement was taken brings the results in excellent agreement with each other.

The main conclusion of this work is that the bias grows monotonically from the present epoch to high redshifts, and the rate at which bias grows increases rapidly as we go towards higher redshifts.

At low redshift the trend of the data-points seems to suggest a bias whose functional form is a weakly increasing function of the redshift. The test-particle bias is a useful model that allows us to predict the evolution of bias for objects that are positively biased. We do not see strong evidence for scale dependent bias or Malmquist effects, but the uncertainties are large.

At higher redshifts the clustering signal appears to come from objects which are highly biased with respect to the underlying distribution of mass. The merging model for the evolution of bias (B2) can correctly describe the steep rise in clustering amplitude seen for $z \gtrsim 2$. We note however that there are several uncertainties in the interpretation of clustering at such redshifts. In particular, at high z we have measurements only for the population of star-forming galaxies, and the lack of reliable absolute magnitude estimates for these objects makes it impossible to apply any quantitative correction for the Malmquist bias.

Lastly we find that the rate at which the observed amplitude decreases at low redshifts is slower than the linear rate of evolution for density perturbations in dark matter in most models. We present arguments which allow us to rule out all models for which this is not the case, i.e. the rate of evolution of galaxy clustering is faster than the linear rate. Present observations do not rule out any model but future observations will allow us to constrain the density parameter. We would like to emphasise that this test does not depend on any detailed modelling of galaxies/halos and so should provide a reliable constraint.

ACKNOWLEDGMENTS

MM acknowledges support from the Isaac Newton Scholarship. Jarle Brinchmann and George Efstathiou are warmly thanked for very helpful and stimulating discussions. We also thank the anonymous referee for comments which improved the content of the paper.

REFERENCES

- Adelberger K.L., Steidel C.C., Giavalisco M., Dickinson M., Pettini M., Kellog M., 1998, *ApJ*, 505, 18
- Arnouts S., Cristiani S., Moscardini L., Matarrese S., Lucchin F., Fontana A., Giallongo E., 1999, *astro-ph/9902290*
- Bagla J.S., 1998, *MNRAS*, 299, 417
- Bardeen J.M., Bond J.R., Kaiser N., Szalay A.S., 1986, *ApJ*, 304, 15
- Baugh C.M., Benson A.J., Cole S., Frenk C.S., Lacey C.G., 1999, *MNRAS*, 305, 21

Blanton M., Cen R., Ostriker J.P., Strauss M.A., 1998, astro-ph/9807029

Brainerd T.G. and Villumsen J.V., 1994, ApJ, 431, 477

Bunn E.F., White M., 1997, ApJ, 480, 6

Carlberg R.G., Cowie L.L., Songaila A., Hu E.M., 1997, ApJ, 484, 538

Carlberg R.G., Yee H.K.C., Morris S.L., Lin H., Sawicki M., Wirth G., Patton D., Shepherd C.W., Ellingson E., Schade D., Pritchet C.J., Hartwick F.D.A., 1998, astro-ph/9805131

Carroll S.M., Press W.H., Turner E.L., 1992, ARA&A, 30, 499

Colin P., Klypin A.A., Kravtsov A.V., Kokhlov A.M., 1998, astro-ph/9809202

Connolly A.J., Szalay A.S., Brummer R.J., 1998, ApJ, 499, L125

Dekel, A., & Lahav, O., 1998, ApJ, submitted (astro-ph/9806193)

Fernandez-Soto A., Lanzetta K.M., Yahil A., 1999, ApJ, 513, 34

Fry J.N., 1996, ApJ, 461, L65

Garilli B., Bottini D., Tresse L., LeFevre O., Saisse M., Vettolani G., 1999, astro-ph/9907320

Giavalisco M., Adelberger K.L., Steidel C.C., Dickinson M., Pettini M., Kellog M., 1998, ApJ, 503, 543

Guzzo L., Strauss M.A., Fisher K.B., Giovanelli R., Haynes M.P., 1997, ApJ, 489, 37

Hamilton A.J.S., Kumar P., Lu E., Mathews A., 1991, ApJ, 374, L1

Hermit S., Santiago B.X., Lahav O., Strauss M.A., Davis M., Dressler A., Huchra J.P., 1996, MNRAS, 283, 709

Huan L., Kirshner R.P., Shectman S.A., Landy S.D., Oemler A., Tucker D.L., Schechter P.L., 1996, ApJ, 471, 617

Jenkins A., Frenk C.S., Pearce F.R., Thomas P.A., Colberg J.M., White S.D.M., Couchman H.M.P., Peacock J.A., Efstathiou G., Nelson A.H., 1998, ApJ, 499, 20

Kaiser N., 1984, ApJL, 284, L9

Kauffmann G., Colberg J.M., Diaferio A., White S.D.M., 1999, MNRAS, 303, 188

Kim R.S.J., Kepner J.V., Strauss M.A., Bahcall N., Gunn J.E., Lupton R.H., Schlegel D.J., 1999, AAS, 194, 8801

Le Fevre O., Hudon D., Lilly S.J., Crampton D., Hammer F., Tresse L., 1996, ApJ, 461, 534

Lahav O., Lilje P.B., Primack J.R., Rees M.J., 1991, MNRAS, 251, 128

Loveday J., Maddox S.J., Efstathiou G., Peterson B.A., 1995, ApJ, 442, 457

Loveday J., Tresse L., Maddox S.J., 1999, in preparation.

Maddox S.J., 1998, 1998yugf.conf..198M

Magliocchetti M., Maddox S.J., Lahav O., Wall J.V., 1999, MNRAS, 306, 943

Magliocchetti M., Maddox S.J., 1999, MNRAS, 306, 988

Matarrese S., Coles P., Lucchin F., Moscardini L., 1997, MNRAS, 286, 115

Mo H., White S.D.M., 1996, MNRAS, 282, 347

Moscardini L., Coles P., Lucchin F., Matarrese S., 1998, MNRAS, 299, 95

Narayanan V.K., Berlind A.A., Weinberg D.H., 1998, submitted to ApJ, astro-ph/9812002

Nusser A., Davis M., 1994, ApJ, 421, L1

Park C., Vogeley M.S., Geller M.J., Huchra J.P., 1994, ApJ, 431, 569

Peacock J.A., Dodds S.J., 1994, MNRAS, 280, L19

Peacock J.A., Dodds S.J., 1996, MNRAS, 267, 1020

Peacock J.A. 1997, MNRAS, 284, 885

Peebles P.J.E., 1980, *The Large-Scale Structure of the Universe*, Princeton University Press

Press W.H., Schechter P., 1974, ApJ, 187, 425

Sheperd C.W., Carlberg R.G., Yee H.K.C., Ellingson E. 1997, ApJ, 479, 82

Saunders W., Rowan-Robinson M., Lawrence A., 1992, MNRAS, 258, 134

Somerville R.S., Primack J.R., 1998, astro-ph/9802268

Sugiyama N., 1995, ApJS, 100, 281

Tegmark M. and Peebles P.J.E. 1998, ApJL 500, L79

Tresse, L., 1999, Les Houches Summer School 1999, astro-ph/9902209

Treyer M.A., Lahav O., 1996 MNRAS, 280, 469

APPENDIX A: USEFUL COSMOLOGICAL QUANTITIES

We express here the quantities appearing in equation 4. Note that $P(\Omega_0, z)$ is obtained by direct integration of the Limber equation (Peebles, 1980).

A1 Case $\Omega_{\Lambda,0} = 0$

$$P(\Omega_0, z) = \frac{\Omega_0^2(1+z)^2(1+\Omega_0 z)^{1/2}}{4(\Omega_0 - 1)[(1+\Omega_0 z)^{1/2} - 1] + \Omega_0^2(1-z) + 2\Omega_0 z}, \quad (\text{A1})$$

$$F(x) = \left[1 - \left(\frac{H_0 x}{c} \right)^2 (\Omega_0 - 1) \right]^{1/2} \quad (\text{A2})$$

$$x = \frac{2c}{H_0} \left[\frac{\Omega_0 z - (\Omega_0 - 2)(1 - \sqrt{1 + \Omega_0 z})}{\Omega_0^2(1+z)} \right], \quad (\text{A3})$$

A2 Case $\Omega_0 + \Omega_{\Lambda,0} = 1$

$$P(\Omega_0, z) = \Omega_0^{1/2} [(1+z)^3 + \Omega_0^{-1} - 1]^{1/2}, \quad (\text{A4})$$

$$F(x) = 1 \quad (\text{A5})$$

$$x = \frac{c}{H_0} \Omega_0^{-1/2} \int_0^z \frac{dz}{[(1+z)^3 + \Omega_0^{-1} - 1]^{1/2}}, \quad (\text{A6})$$